Robotica (2015) volume 33, pp. 898–919. © Cambridge University Press 2014
doi:10.1017/S0263574714000617

Post-capture attitude control for a tethered space robot–target combination system

Panfeng Huang*, Dongke Wang, Zhongjie Meng and Zhengxiong Liu

National Key Laboratory of Aerospace Flight Dynamics, Northwestern Polytechnical University, Xi'an 710072, P.R. China
Research Center for Intelligent Robotics, School of Astronautics, Northwestern Polytechnical University, Xi'an 710072, P.R. China

(Accepted February 13, 2014. First published online: March 20, 2014)

SUMMARY
This paper presents a novel scheme for achieving attitude control of a tumbling combination system in the post-capture phase of a tethered space robot (TSR). Given the combination rotation characteristics, tether force is applied to provide greater control torques for stabilising the attitude. The proposed control scheme involves two attitude controllers, which coordinate the controller of the tether force and thruster force and the controller of single thruster force. The numerical simulations include a comparison between this coordinated control and the traditional thruster control and a sensitivity analysis on initial values of parameters. Simulation results validate the feasibility of the attitude control scheme for a tumbling combination system, and fuel consumption of the attitude control is efficiently reduced using the coordinated control strategies.

KEYWORDS: Tethered space robot; Post-capture; Combination system attitude control; Coordinated control; Switching control.

1. Introduction

Tethered Space Robot (TSR) systems consist of a gripper, a space tether and a space platform (Fig. 1) for future use in on-orbit services, including on-orbit maintenance, on-orbit refuelling, auxiliary orbit transfer and space debris removal.[1–3] Many problems may arise during the different phases of a TSR capture mission, which is typically divided into the deployment, approach, capture and post-capture phases. Research into the issues of deployment and capture control can be found in the literature.[4–8]

The attitude control of a tethered system in space has received extensive attention with several papers published on the subject in recent years. Nohmi[9–11] investigated the arm link to control the TSR's attitude during the deployment phase, and a microgravity experiment was conducted to validate the feasibility of this scheme. Godard and Kumar[12] designed a nonlinear optimal controller using an inverse optimal technique to control the attitude of a satellite via tether-offset variations. The attitude of the mother satellite is controlled by four tethers, which are connected with the sub-satellite as described in the literature.[13] Beda[14] investigated how the attitude dynamics of a tethered satellite can be controlled for eccentric orbits by simply using the feedback of a pitch angle. The tether tension/length control law was designed to control the attitude of a tethered satellite formation as described in the literature.[15] Chang *et al.*[16] analysed the attitude dynamics and control of a three-inline tethered satellite flying formation, and the state-dependent Riccati equation controller was used to regulate attitude errors. Menon and Bombardelli[17] proposed a method to control the position and attitude of two tethered units using two passive dampers placed at the tether attachment point. Bergamaschi and Bonon[18] studied the coupling between the tether taut string vibrations and the satellite attitude motion.

* Corresponding author. E-mail: pfhuang@nwpu.edu.cn

https://doi.org/10.1017/S0263574714000617 Published online by Cambridge University Press

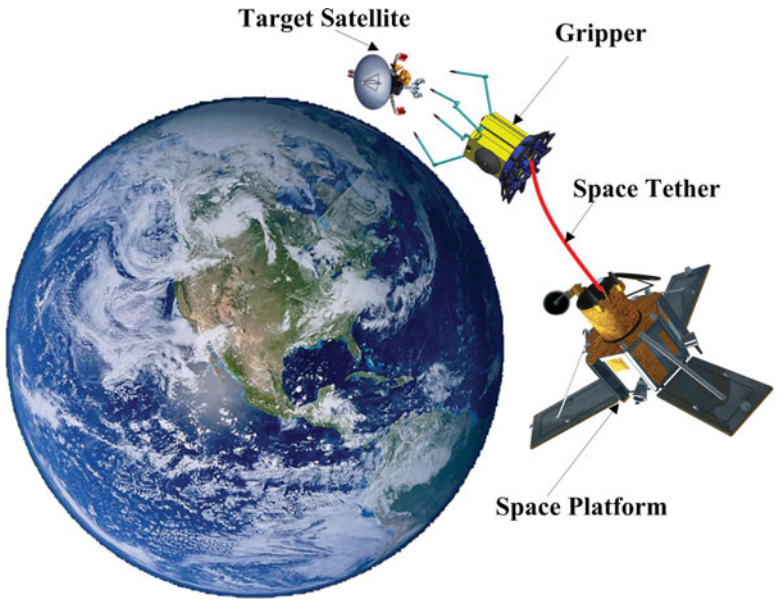


Fig. 1. TSR system.

The capture and post-capture control of a traditional space robot has been studied by many researchers. Yoshida *et al.*[19] proposed a possible control sequence that included the bias momentum approach during the approaching phase, the impedance control during the impact phase and the distributed momentum control during the post-impact phase for a successful capturing operation. Flores-Abad and Ma[20] proposed an optimal control strategy for a space manipulator to provide minimal impact to the base satellite during a capturing operation. Liu *et al.*[21] derived an impact model to simulate the post-impact dynamics of the entire system and designed a proportional derivative (PD) controller to maintain the stabilisation of the robot system after the capture of the object. Chau *et al.*[22] presented a trajectory generation algorithm for a space manipulator after capturing an uncooperative tumbling target. Aghili[23,24] focused on controlling the space manipulator in the post-capture phase to bring a tumbling satellite to rest. Xu *et al.*[25] proposed a method for berthing a target and re-orientating the base using manipulator motion only after the capture.

In addition, Nakamura *et al.*[26] investigated the collaborative control of the tension and thruster primarily during the approach phase to the target. Spencer *et al.*[27] compared the dynamics and control of a space robot subjected to a tether tension force with those for a free-floating space robot.

After a target is captured by a TSR, the gripper and target form a new combination system. The dynamic characteristics of the combination system differ from those of a TSR in its deployment, approach or capture phase. Due to the presence of the space tether, the post-capture dynamic characteristics of the combination system can be distinguished from the aforementioned characteristics of a traditional space robot. The collision during the capture and the original target rotation lead to the tumbling of the combination, which could cause the tether to become tangled with the combination and influence the security of the space platform.

The attitude control of the combination can hardly be achieved by the thrusters of the gripper alone, because the control torque of the thrusters and the fuel of the gripper are limited. In the above-mentioned existing literature, tether is usually used to provide tension to control relative positions of satellite formation or the positions of space robots during the phase of release towards the target. However, the space tether can also provide great control torques for the attitude control. Therefore, this work aims to design an attitude-coordinated controller of the tether and the thrusters to stabilise the TSR–target combination system and reduce the fuel consumption at the same time.

This paper consists of four main sections. Section 2 utilises the Euler formulation approach to obtain the dynamics equations of motion for the combination system and analyses the dynamic characteristics. In Section 3, the parameter identification is first used to acquire inertia matrix and centroid position of the combination system. Tether force is applied to control the combination attitude with thruster force, and two simple coordinated controllers are derived for the combination. These

https://doi.org/10.1017/S0263574714000617 Published online by Cambridge University Press

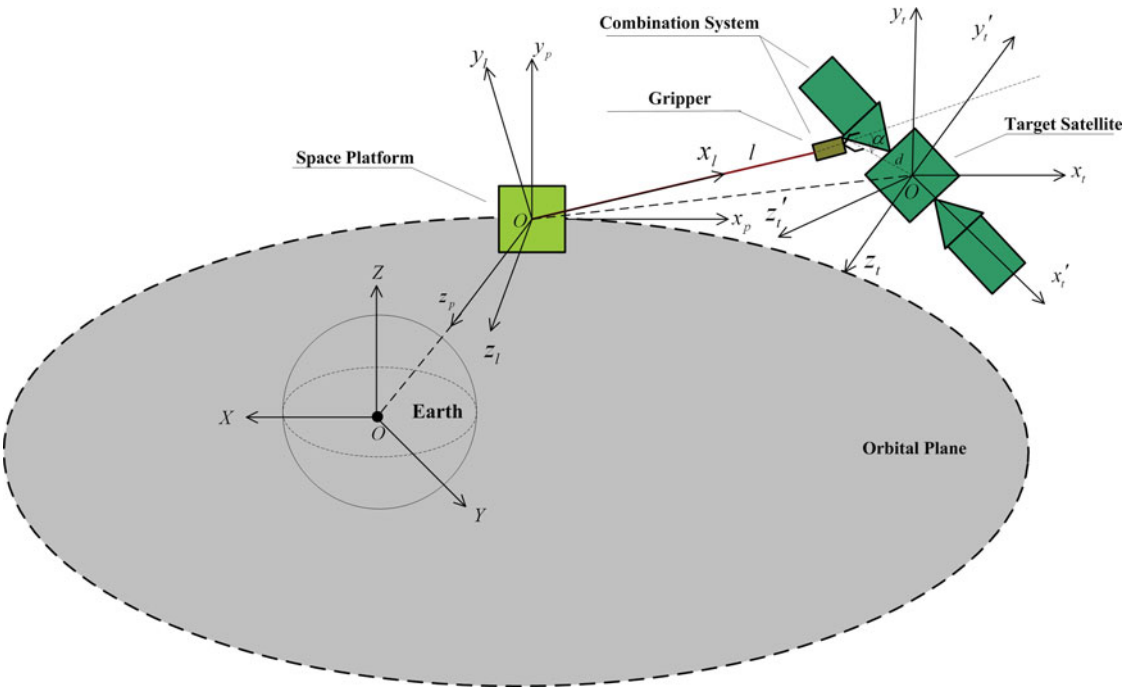


Fig. 2. Target capture of a TSR.

coordinated controllers are utilised according to the switching conditions, which are optimised via genetic algorithm. In Section 4, the feasibility of the control scheme is validated using a numerical simulation, and the results are presented and analysed. The conclusions are discussed in Section 5.

2. Dynamics Model

2.1. Task description

As shown in Fig. 2, due to the spinning of the target and the collision between the gripper and the target, the gripper rotates along with the target after the capture, and the combination system consists of gripper and target. The origin of the platform orbital frame, $Ox_py_pz_p$, is located at the centroid of the space platform. The axes of the coordinate are oriented as follows: The x-axis is in the orbital plane in the local horizontal direction, the y-axis is along the orbital normal and the z-axis is collinear with the line that extends from the centre of the Earth to the centroid of the space platform and completes a right-handed triad. Given flying-around distance for the platform observing the target before the capturing mission and the limited fuel of the gripper for the capturing mission, the tether is assumed to be a few hundred metres long in this paper. Therefore, $Ox_ty_tz_t$ denotes the combination orbital frame that is approximately parallel with $Ox_py_pz_p$; $Ox_ly_lz_l$ is the tether frame with its x-axis along the tether direction, and $Ox'_ty'_tz'_t$ is the combination body frame.

The following assumptions are made:

1. The tether is inelastic and massless. Compared with space platform or robot–target combination at hundreds or thousands of kilograms level, the mass of the tether at a hundred-metre level is relatively small and could be neglected. For example, the density of the Kevlar tether[28] (1-mm diameter) used for European Space Agency's (ESA) ROGER project is 4.5 kg/km, and the mass of 1-km tether here is only 4.5 kg. Therefore, the influence of tether to the issue discussed herein can be neglected and the tether is assumed to be massless.
2. No time delay exists in the tension transmission along the space tether and force feedback of tether reel, and the vibration of the space tether is neglected. Moreover, no tension exists when the space tether is slack.

https://doi.org/10.1017/S0263574714000617 Published online by Cambridge University Press

3. The target is firmly captured with no sway of solar paddle or other unstable phenomena occurring during the attitude control.
4. The platform can endure the influence of tether tension from its own thrusters, and its position and attitude can be maintained during the coordinated attitude control of the combination system.

2.2. Attitude dynamics model

Assuming the combination system is a rigid body, its attitude dynamics equation can be given by the following equation:

$$J\dot{\omega} = -\omega^{\times} J\omega + T_c + T_l + T_d, \tag{1}$$

where $\omega = [\,\omega_1\ \omega_2\ \omega_3\,]^T \in R^3$ denotes the absolute angular velocity of the combination expressed in the body frame $Ox_t'y_t'z_t'$, $J \in R^{3\times3}$ is the inertia matrix of the combination and $J = J_0 + \Delta J$ with J_0 as the nominal value and ΔJ is the bounded uncertainty due to the thruster consumption; $T_c \in R^3$denotes the control torque of the gripper and is equivalently realized via pulse-width-modulation (PWM) thrusters.

$T_l \in R^3$ denotes the control torque of the tether, and $\omega^{\times}$ is the skew-symmetric matrix of ω defined as follows:

$$\omega^{\times} = \begin{pmatrix} 0 & -\omega_3 & \omega_2 \\ \omega_3 & 0 & -\omega_1 \\ -\omega_2 & \omega_1 & 0 \end{pmatrix}.$$

$T_d \in R^3$ is the attitude disturbance torque, which is caused by the thruster force of the gripper. The target is assumed to have no capacity for orbit control, and the gripper's thrusters are utilised to control the combination orbit. The gripper is not located in the centroid of the combination and the vector of the control force does not extend through the centroid of the combination, therefore T_d is generated.

The Modified Rodrigues Parameter (MRP)[29] is adopted to describe the kinematics model of the combination attitude as follows:

$$\dot{\sigma} = G(\sigma)\omega, \tag{2}$$

where $\sigma = [\,\sigma_1\ \ \sigma_2\ \ \sigma_3\,]^T \in R^3$, and $G(\sigma)$ is defined as follows:

$$G(\sigma) = \frac{1}{4}\left[(1-\sigma^T\sigma)I + 2\sigma^{\times} + 2\sigma\sigma^T\right], \tag{3}$$

where I is a 3×3 unit matrix.

The transformation matrix from the platform orbital frame to the combination body frame is:

$$R = I_3 - \frac{4(1-\sigma^2)}{(1+\sigma^2)^2}\left[\sigma^{\times}\right] + \frac{8}{(1+\sigma^2)^2}\left[\sigma^{\times}\right]^2. \tag{4}$$

Assuming that the transformation matrix from the platform orbital frame to the tether frame isR_{lp}, the transformation matrix R_{bl} from the tether frame $Ox_ly_lz_l$ to the combination body frame $Ox_t'y_t'z_t'$ is given by:

$$R_{bl} = RR_{lp}^{-1}. \tag{5}$$

For convenience, the relative attitude angles from the tether frame $Ox_ly_lz_l$ to the combination body frame $Ox_t'y_t'z_t'$ are defined by the Euler angle, the roll angle ϕ, the pitch angle θ and the yaw angle ψ of the 1-2-3 Euler rotation sequence. The term R_{bl} can be expressed by ϕ, θ and ψ as follows:

$$R_{bl} = \begin{bmatrix} \cos\psi\cos\theta & \cos\psi\sin\theta\sin\phi + \sin\psi\cos\phi & -\cos\psi\sin\theta\cos\phi + \sin\psi\sin\phi \\ -\sin\psi\cos\theta & -\sin\psi\sin\theta\sin\phi + \cos\psi\cos\phi & \sin\psi\sin\theta\cos\phi + \cos\psi\sin\phi \\ \sin\theta & -\cos\theta\sin\phi & \cos\theta\cos\phi \end{bmatrix}. \tag{6}$$

https://doi.org/10.1017/S0263574714000617 Published online by Cambridge University Press

By combining Eqs. (5) and (6), the three Euler angles ϕ, θ and ψ can be obtained as

$$\begin{cases} \theta = \arcsin(R_{bl}(3,1)), \\ \phi = \arctan\left(-\frac{R_{bl}(3,2)}{R_{bl}(3,3)}\right), \\ \psi = \arctan\left(-\frac{R_{bl}(2,1)}{R_{bl}(1,1)}\right). \end{cases} \tag{7}$$

2.3. Error attitude dynamics model

The error attitude MRP σ_e and the error attitude angular velocity ω_e of the body frame are defined as follows[30]:

$$\begin{cases} \sigma_e = \sigma \otimes \sigma_d^{-1}, \\ \omega_e = \omega - \omega_d, \end{cases} \tag{8}$$

where ω_d denotes the desired angular velocity in the body frame, and σ_d is the desired attitude. The symbol $\otimes$ denotes the MRP multiplication, which can be defined as follows:

$$\sigma_1 \otimes \sigma_2^{-1} = \frac{(1-\sigma_2^T\sigma_2)\sigma + (\sigma_1^T\sigma_1 - 1)\sigma_2 - 2\sigma_2 \times \sigma_1}{1 + (\sigma_2^T\sigma_2)(\sigma_1^T\sigma_1) + 2\sigma_2^T\sigma_1}. \tag{9}$$

By substituting Eq. (8) into Eq. (1), the error attitude dynamics equation and the kinematics equation can be obtained:

$$\begin{cases} \dot{\sigma}_e = G(\sigma_e)\omega_e, \\ J\dot{\omega}_e = -\omega^{\times} J\omega - JR\dot{\omega}_d + T_c + T_l + T_d. \end{cases} \tag{10}$$

2.4. Orbit dynamics model

The Hill equation is adopted to represent the orbit motion of the combination system:

$$\begin{cases} \ddot{x} - 2n\dot{z} = a_x + a_{tx} - n^2\varepsilon_x \\ \ddot{y} + n^2 y = a_y + a_{ty} - n^2\varepsilon_y \\ \ddot{z} + 2n\dot{x} - 3n^2 z = a_z + a_{tz} - n^2\varepsilon_z \end{cases}, \tag{11}$$

where $[\,x\ y\ z\,]^T \in R^3$ is the centroid position of the combination in the platform orbital frame $Ox_py_pz_p$, n denotes the mean orbital angular velocity, $[\,a_x\ a_y\ a_z\,]^T \in R^3$ denotes the linear acceleration of the gripper's thruster force and $[\,a_{tx}\ a_{ty}\ a_{tz}\,]^T \in R^3$ denotes the linear acceleration due to tether tension. Assuming the target has no orbital control capacity, the orbit of the combination system can only be controlled by the thrusters of the gripper or possibly by the thrusters and the tether tension together.

Define the position vector of the capture position in the combination body frame as d, and the tether tension as F_l. A tether tension that is too great can strongly influence the space platform and even cause instability throughout the system; therefore, F_l should satisfy the following constraint:

$$F_l \le F_{l\max}, \tag{12}$$

Hence, the tether tension vector in the platform frame $Ox_py_pz_p$ can be written as:

$$F = -\frac{[x,y,z]^T + R^{-1}d}{\left\|[x,y,z]^T + R^{-1}d\right\|}F_l. \tag{13}$$

https://doi.org/10.1017/S0263574714000617 Published online by Cambridge University Press

The linear accelerations caused by the tether tension are given by:

$$[\,a_{tx} \quad a_{ty} \quad a_{tz}\,]^T = -\frac{[x, y, z]^T + R^{-1}d}{\left\|[x, y, z]^T + R^{-1}d\right\|} \cdot \frac{F_l}{m}, \tag{14}$$

where m is the mass of the combination system.

Multiplying by the transformation matrix R, the tether force in the combination body frame can be obtained, and the tether control torque can be acquired:

$$T_l = d \times (RF). \tag{15}$$

2.5. Dynamics analysis

The gripper rotates together with the target after the capture. The thruster force and the tether tension are utilised to control the combination attitude. By setting the left side of Eq. (15) T_l to be zero yields the following:

$$(RF) \times d = 0.$$

The tether torque has no influence on the combination attitude when the tether vector is collinear with d; the tether vector goes through the centroid of the combination. The corresponding attitude is chosen as the desired attitude, $\sigma_d = [\,\sigma_{d1} \quad \sigma_{d2} \quad \sigma_{d3}\,]^T$. This definition has remarkable advantages; if the desired states are not σ_d, the combination will sway and even become unstable when retrieved due to the tether tension torque or deorbited to another orbit after the combination attitude is stabilised. The value of σ_d changes with the position of the combination system and can be deduced as follows.

The unit vector of the tether vector in the platform orbital frame is $\frac{[x,y,z]+R^{-1}d}{\|[x,y,z]+R^{-1}d\|}$. When the desired attitude is obtained, the tether frame $Ox_l y_l z_l$ is parallel to the combination body frame $Ox'_t y'_t z'_t$, and the orientation of the tether follows the Ox'_t axis. The unit vector of the tether in the tether frame is $[1, 0, 0]^T$, and the transformation matrix from the platform to the tether frame is R_{lp}, then the following relationship is satisfied:

$$[1, 0, 0]^T = R_{lp}\frac{[x, y, z]^T + R^{-1}d}{\left\|[x, y, z]^T + R^{-1}d\right\|}. \tag{16}$$

Equating Eq. (16) yields

$$R_{lp} = [1, 0, 0]^T\left(\frac{[x, y, z]^T + R^{-1}d}{\left\|[x, y, z]^T + R^{-1}d\right\|}\right)^+, \tag{17}$$

where $()^+$ is the Moore–Penrose inverse.

From the transformation matrix R_{lp}, the rotating angle α and the Euler axis $e = (\,e_x \; e_y \; e_z\,)^T$ are given by:

$$\begin{cases} \cos\alpha = (R_{lp11} + R_{lp22} + R_{lp33} - 1)/2 \\ e_x = (R_{lp23} - R_{lp32})/(2\sin\alpha) \\ e_y = (R_{lp31} - R_{lp13})/(2\sin\alpha) \\ e_z = (R_{lp12} - R_{lp21})/(2\sin\alpha) \end{cases}. \tag{18}$$

According to the MRP definition, σ_d is obtained as follows:

$$\sigma_d = \tan\frac{\alpha}{4}e. \tag{19}$$

In addition, the desired angular velocity is defined as: $\omega_d = [\,0 \quad 0 \quad 0\,]^T$.

https://doi.org/10.1017/S0263574714000617 Published online by Cambridge University Press

3. Coordinated Control Strategies

When capture of the target is complete, the traditional thruster control to the combination attitude alone can lead to the following cases:

1. The combination attitude cannot be stabilised quickly because the control torque of the gripper is limited, and the tether may eventually become intertwined with the combination. This serious situation is very dangerous and the platform could even be threatened for the existence of space tether.
2. The combination attitude can be stabilised by the thruster control; however, the fuel consumption is too high.

As a result, the attitude control of the TSR–target combination can hardly be achieved by the traditional thruster control alone as the fuel consumption of the thruster control alone is too high. Considering that the tether could provide considerable control torque, the design of the attitude-coordinated controller using the tether tension and the thruster force is discussed in this study. The tether tension could lead to a change in the combination position; however, the attitude control is more urgent and important than the position control because the spinning of the combination will cause the tether to become intertwined and can even cause instabilities of the platform and the entire system, whereas a change in the position of the combination does not have a great influence.

The chosen desired attitude σ_d varies with the combination position, but the position control will not be discussed here. Furthermore, the combination position is assumed to be without control for simplicity and convenience of the attitude controller design; therefore, T_d and $[\, a_{tx}\ a_{ty}\ a_{tz}\,]^T$ are set to zero.

The inertial matrix and the centroid position of the combination system are as yet unknown. Therefore, the parameters are identified prior to the controller design. Considering the attitude characteristics of the combination, the coordinated controller is designed to consist of two attitude controllers, which are used according to the switching conditions. During the initial stage of the attitude control, the pitch and yaw motion of the combination are controlled via tether because it can provide greater torque of these two axes than gripper thrusters. Meanwhile, the roll motion is controlled by the thruster. The attitudes of the three axes are primarily controlled by the tether tension and the thruster. When the pitch and yaw attitude are stabilised within a certain range, the controller is switched to the thruster control only because the smaller pitch and yaw angles lead to a smaller torque arm, and greater tether tension is necessary to obtain the required torque. Greater tether tension will obviously cause a greater influence over the position of the combination; thus, an increased tether tension is unfeasible and should be avoided. Moreover, the thruster control could achieve high accuracy attitude control, which is preferred. In addition, the switching conditions are optimised using the genetic algorithm to ensure the stability and convergence of controller and reduce fuel consumption. The exact design steps of coordinated controllers are described in the following section.

3.1. Parameter identification

The inertia matrix and centroid position of the post-capture combination system are unknown, but these are necessary for the design of attitude controller. Therefore, these parameters are identified according to the following steps.

Combining Eqs. (10) and (15) yields

$$J\dot{\omega}_e = -\omega^{\times} J\omega - JR\dot{\omega}_d + T_c + (RF) \times d, \tag{20}$$

where $F = -\frac{[x,y,z]^T + R^{-1}d}{\|[x,y,z]^T + R^{-1}d\|} F_l$ is the tether tension vector, the tether tension F_l is measurable, and $[x, y, z]^T + R^{-1}d$ denotes the capture position, which can be computed from gripper's measurable centroid position. Assume the relative position between the platform and the gripper can be measured to very high accuracy, which is at least a few centimeters for the case of a hundred-metre distance.

Assuming that the centroid position and the capture position in the combination body frame are Δd and d_0, respectively, the following relation can be obtained:

$$d = d_0 - \Delta d. \tag{21}$$

https://doi.org/10.1017/S0263574714000617 Published online by Cambridge University Press

Equation (20) can be written as:

$$J\dot{\omega}_e + \omega^{\times} J\omega + JR\dot{\omega}_d + (RF)^{\times}\Delta d = T_c + (RF)^{\times} d_0. \tag{22}$$

The parameters to be identified are:

$$\theta = \begin{pmatrix} J_{11} & J_{12} & J_{13} & J_{21} & J_{22} & J_{23} & J_{31} & J_{32} & J_{33} & \Delta d_1 & \Delta d_2 & \Delta d_3 \end{pmatrix}^T.$$

Equation (22) could be rearranged in the following form:

$$T = \Phi\theta, \tag{23}$$

where

$$T = T_c + (RF)^{\times} d_0,\ \Phi = \begin{pmatrix} \Phi_1 \\ \Phi_2 \end{pmatrix}^T,\ \Phi_1 = \begin{pmatrix} \Phi_{11} & \omega_1\omega_3 & -\omega_1\omega_2 \\ \Phi_{21} & \omega_2\omega_3 & -\omega_2^2 \\ \Phi_{31} & \omega_3^2 & -\omega_2\omega_3 \\ -\omega_1\omega_3 & \Phi_{24} & \omega_1^2 \\ -\omega_2\omega_3 & \Phi_{25} & \omega_1\omega_2 \\ -\omega_3^2 & \Phi_{26} & \omega_1\omega_3 \\ \omega_1\omega_2 & -\omega_1^2 & \Phi_{37} \\ \omega_2^2 & -\omega_1\omega_2 & \Phi_{38} \\ \omega_2\omega_3 & -\omega_1\omega_3 & \Phi_{39} \end{pmatrix}^T,\ \Phi_2 = \left((RF)^{\times}\right)^T.$$

The elements of Φ_1 are as follows:

$$\begin{cases} \Phi_{11} = \Phi_{24} = \Phi_{37} = \dot{\omega}_{e1} + R_{11}\dot{\omega}_{d1} + R_{12}\dot{\omega}_{d2} + R_{13}\dot{\omega}_{d3} \\ \Phi_{21} = \Phi_{25} = \Phi_{38} = \dot{\omega}_{e2} + R_{21}\dot{\omega}_{d1} + R_{22}\dot{\omega}_{d2} + R_{23}\dot{\omega}_{d3} \\ \Phi_{31} = \Phi_{26} = \Phi_{39} = \dot{\omega}_{e3} + R_{31}\dot{\omega}_{d1} + R_{32}\dot{\omega}_{d2} + R_{33}\dot{\omega}_{d3} \end{cases}.$$

Assuming that the angular velocity ω and the angular acceleration $\dot{\omega}_e$ of the parameter matrix can be measured using a gyro compass, the value of σ_e can be obtained visually; therefore, R_{lp}, R_{bl} and R can be acquired indirectly via computation. In addition, the inputs T_c and T_l are known and available.

The formulations of the identification based on the least-squares method are:

$$\begin{cases} \hat{\theta}(k) = \hat{\theta}(k-1) + K(k)[y(k) - \Phi(k)\hat{\theta}(k-1)] \\ K(k) = P(k-1)\Phi^T(k)[I + \Phi(k)P(k-1)\Phi^T(k)]^{-1} \\ P(k) = [I - K(k)\Phi(k)]P(k-1) \end{cases}. \tag{24}$$

The identification algorithm is implemented according to the following steps:

1. Set the initial values of $\hat{\theta}(k)$ and$P(k-1)$.
2. Obtain the required sampled data, including ω, $\dot{\omega}_e$, T_c, T_l etc.
3. Calculate $K(k)$, $\hat{\theta}(k)$ and $P(k)$ using Eq. (32).
4. Set $k = k + 1$ and return to step (2) until the simulation is terminated.

3.2. Coordinated controller of tether and thrusters

The tether tension could provide two axes of torque to control the pitch angle θ_e and the yaw angle ψ_e. However, only the variable F_l is available for the controller design. Hence, for a convenient controller design, we must find a single variable to denote both pitch and yaw angles. As shown in Fig. 1, to eliminate the attitude errors, θ_e and ψ_e, is actually to control the capture position vector $\boldsymbol{d}$ and the tether tension vector $\boldsymbol{F}$ so that the tether vector goes through the centroid of the combination. In this case, $\boldsymbol{d}$ and $\boldsymbol{F}$ are collinear. Therefore, the variable corresponding to the pitch and yaw angles could

https://doi.org/10.1017/S0263574714000617 Published online by Cambridge University Press

be the angle between d and F, which is defined as η and given by:

$$\eta = \arccos\left(\frac{F^T(R^{-1}d)}{|F|\left|R^{-1}d\right|}\right). \tag{25}$$

The PD controller is adopted to control pitch and yaw motions via η. The tether tension vector F could be measured, R could be computed from the attitude and the value of d could be determined as identified in Section 3.4; therefore, the value of η is available. The tether tension is given by

$$F_l = \begin{cases} (k_{pl} + k_{dl}S)\eta & (k_{pl} + k_{dl}S)\eta \geq 0 \\ 0 & (k_{pl} + k_{dl}S)\eta < 0 \end{cases}, \tag{26}$$

where k_{pl} denotes the proportional coefficient, and k_{dl} is the damping coefficient. The tether tension F_l must be positive.

By combining Eqs. (13) and (15), the control torque T_l can be obtained:

$$T_l = \left[R\left(\frac{[x, y, z]^T + R^{-1}d}{\left\|[x, y, z]^T + R^{-1}d\right\|}F_l\right)\right] \times d. \tag{27}$$

The tether could only provide two axes of attitude torque, and the roll motion could only be controlled by the thruster force. In addition, the roll motion exerts too great an influence on the other two motions, so the PD controller is adopted to stabilise the roll motion,

$$T_c(1) = k_{pc}\phi_e + k_{dc}\omega_{ex}. \tag{28}$$

The terms $\theta_e$and ψ_e can be obtained from Eqs. (7) and (8), and k_{pc} and k_{dc} denote the proportional coefficient and the damping coefficient respectively.

As a result, the coordinated controller of the tether tension and thruster force is composed by Eqs. (22) and (23).

3.3. Thruster controller design

When the pitch and yaw error attitudes are controlled within a certain range, the controller is switched to the thruster control only. Although an inertia matrix is acquired by the parameter identification, errors in the identified and actual values still exist, which can lead to instability in the control system. The sliding mode control approach is recognised as an efficient tool for designing robust controllers for nonlinear dynamic plants under uncertainty conditions. Therefore, sliding mode control is adopted to reduce the influence of uncertainty in the inertial matrix and other disturbances.

The error attitude dynamics equation is given by Eq. (10). The sliding surface is defined as $s = \omega_e + c\sigma_e$, where $c > 0$. The sliding mode controller is designed as

$$T_c = \omega^{\times} J\omega + J\dot{\omega}_d - cJG(\sigma_e)\omega_e - \lambda \mathrm{sgn}(s) \tag{29}$$

with $\lambda > 0$.

Choosing $V = \frac{1}{2}\boldsymbol{s}^T \boldsymbol{J} s$ as the Lyapunov function, the time derivative of $V$is

$$\begin{aligned} \dot{V} &= s^T J\dot{s} \\ &= s^T J(\dot{\omega}_e + c\dot{\sigma}_e). \end{aligned} \tag{30}$$

By substituting Eq. (10) into Eq. (14), one can obtain

$$\dot{V} = s^T(T_c - \omega^{\times} J\omega - J\dot{\omega}_d + cJG(\sigma_e)\omega_e) = s^T[-\lambda \mathrm{sgn}(s) + f(\Delta J)],$$

where $f(\Delta J) = -\omega^{\times}\Delta J\omega - \Delta J\dot{\omega}_d + \Delta JG(\sigma_e)\omega_e$. The term ΔJ, which is due to fuel consumption, is bounded, implying that $f(\Delta J)$ is also bounded. Assuming $\{\begin{smallmatrix}\Delta_{\max} = \|f(\Delta J)\|_{\infty} \\ f(\Delta J) = [\,\Delta_1\ \ \Delta_2\ \ \Delta_3\,]^T\end{smallmatrix}$ and setting $\lambda =$

https://doi.org/10.1017/S0263574714000617 Published online by Cambridge University Press

$\Delta_{\max} + \delta$, in which δ is an arbitrary positive number, one can derive:

$$\begin{aligned}
\dot{V} &= \sum_{i=1}^{3} s_i^T [-(\Delta_{\max} + \delta)\mathrm{sgn}(s_i) + \Delta_i] \\
&= \sum_{i=1}^{3} s_i^T [-\delta \mathrm{sgn}(s_i) - \Delta_{\max}\mathrm{sgn}(s_i) + \Delta_i] \\
&= -\sum_{i=1}^{3} s_i^T \delta \mathrm{sgn}(s_i) + \sum_{i=1}^{3} [-\Delta_{\max} s_i^T \mathrm{sgn}(s_i) + \Delta_i s_i^T] \\
&\leq -\sum_{i=1}^{3} s_i^T \delta \mathrm{sgn}(s_i) \\
&\leq 0.
\end{aligned}$$

$V > 0$ and $V \leq 0$, so it is believed that asymptotically stable system meets the sliding condition.

There must be chattering in the control system for the existence of a sign function in Eq. (29). To solve this problem, the sign function can be modified into saturation functions:

$$\mathrm{sat}(s_i, \varepsilon) = \begin{cases} 1 & s_i > \varepsilon \\ s_i/\varepsilon & -\varepsilon \leq s_i \leq \varepsilon \\ -1 & s_i < -\varepsilon \end{cases}, \tag{31}$$

where $i = 1, 2, 3$, and ε is a positive number.

3.4. Switching conditions and parameter optimisation

When using the tether tension to control the pitch θ and yaw ψ angles, one expects to make full use of the tether tension when both θ and ψ are relatively large, and to utilise the thruster force to stabilise the angles and achieve high attitude control accuracy when these are relatively small. Therefore, the pitch θ and yaw ψ angles are chosen as the switching conditions of a coordinated controller and a thruster controller respectively. The switching conditions are given by

$$\begin{cases} |\psi| \leq \psi_s, \\ |\theta| \leq \theta_s, \end{cases} \tag{32}$$

where ψ_s and θ_s are the switching angles, and both are subject to constants. When the conditions in Eq. (32) are satisfied, Eq. (24) is utilised. In contrast, when any of these conditions is not satisfied, Eqs. (22) and (23) are utilised.

Angles ψ_s and θ_s have remarkable effects on the coordinated control performance. Thus, one expects to find the optimal values of ψ_s and θ_s, which can optimise performance of the control index. The optimisation of ψ_s and θ_s is actually a problem of optimisation with constraints because the optimal values should enable the system to work with the lowest possible fuel consumption, whereas the constraints on the control input should always be satisfied. This parameter optimization problem could not be solved in an analytical way, for it does not work with attitude tracking control problem because of its complexity. The genetic algorithm should be resorted to solve this constraint-submitted nonlinear parameter optimisation problem. In this case, an index for evaluating the performance of the system is defined as follows:

$$J_1 = k_1 \int_0^{t_f} T_c^T T_c dt + k_2 \int_0^{t_f} F^T F dt + k_3 \int_0^{t_f} \sigma_e^T \sigma_e dt, \tag{33}$$

where the first term on the right side is the weighted fuel consumption, the second is the weighted position influence of the tether tension for the combination system and the third term is the penalty

https://doi.org/10.1017/S0263574714000617 Published online by Cambridge University Press

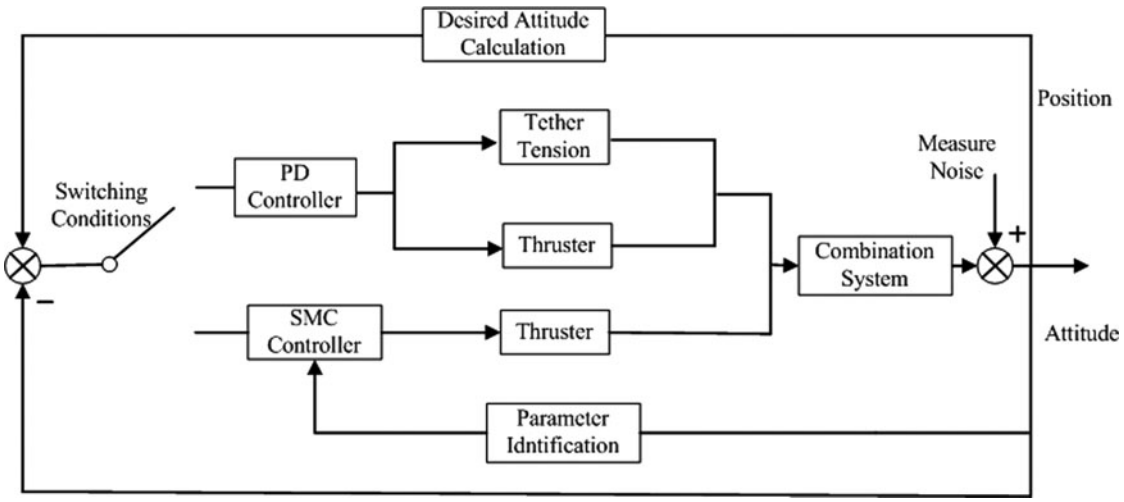


Fig. 3. Block diagram of coordinated controllers.

term, which can enhance the convergence speed and guarantee the stability of the combination system. However, improper switch values of ψ_s and θ_s angles can lead to instability of the system. Terms k_1, k_2 and k_3 are their weights.

The genetic algorithm is implemented in the following steps[31]:

1. Choose search sets for both ψ_s and θ_s, encode them as n-bit binary strings and generate the initial population with N_p individuals.
2. Calculate the fitness value for each individual according to Eq. (28).
3. From the current population, select the strings with probabilities proportional to their fitness values.
4. The single-point crossover operation is performed on the selected strings with a probability of P_x.
5. A mutation is then applied to new chromosomes with a set probability of P_m. The new generation has now been completed.
6. Evaluate the new generation using Eq. (28), and repeat steps (3)–(6) until N_g generations are achieved.

Figure 3 shows the block diagram of the coordinated attitude controller for the TSR–target combination.

4. Numerical Simulation

Numerical simulations are first carried out to compare the performance of the coordinated controller with that of the traditional thruster controller in Section 4.1. In order to further investigate the feasibility of this coordinated control scheme, a simplified sensitivity analysis for different initial conditions of the combination is conducted in Section 4.2.

4.1. Comparison of coordinated control and traditional thruster control

Table I shows the initial values of the parameters. Assuming that the -V-bar capture is adopted and the initial position of the combination is (200, 0, 0) m, the initial angular velocities of the three axes of the combination are 10° /s. Thrusters are assumed to have a constant control torque of 5 Nm when corresponding thrusters are turned on and work in the PWM mode with a control cycle of 250 ms. In addition to the simulation of the coordinated controller, the sliding mode controller of the thruster force only (traditional thruster control) is also simulated, and the result is compared with the former.

https://doi.org/10.1017/S0263574714000617 Published online by Cambridge University Press

Table I. Initial value of the parameters.

Parameters	Initial values
σ_e	(0.0999, 0.2015, 0.1008)
ω_e	(10, 10, 10)° /s
c	1
$[x\ y\ z]^T$	(200, 0, 0) m
$[\dot{x}\ \dot{y}\ \dot{z}]^T$	(0, 0, 0) m/s
n	0.0011 rad/s

Table II. Optimal values of switching conditions.

Parameters	Optimal values
ψ_s	29.23°
θ_s	11.85°

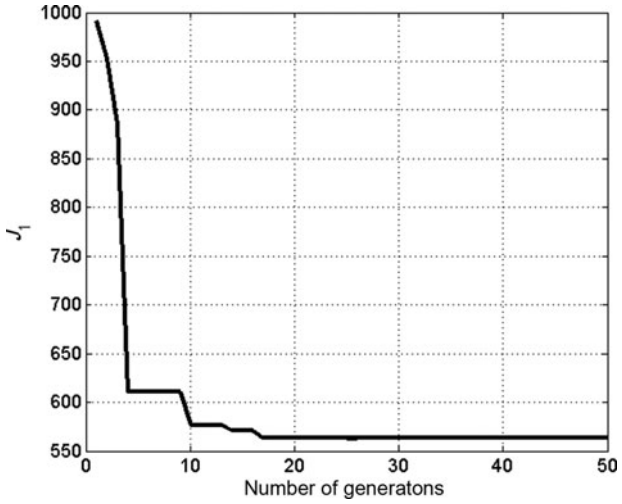


Fig. 4. Value of J_1 with respect to the number of generations.

Figure 4 provides the optimisation result for J_1, in which $k_1 = 0.7$, $k_2 = 0.2$, $k_3 = 0.1 \times 100$. The multiplied coefficient 100 of k_3 increases the influence of the third J_1 term, and if $k_3 = 0.1$, the third term is too small to ensure the convergence of the system. At 567.5, J_1 converges after 17 generations. As shown in Table II, the optimal values of the switching condition are $\psi_s = 29.23°$, $\theta_s = 11.85°$.

Figure 5 shows the identification results of the inertial matrix J, and that the maximum identification errors of J_{11}, J_{22} and J_{33} are 7.10%, 8.79% and 2.54%, respectively, which are less than 10%. The J_{21} has a maximum identification error of 12.1 kg m^2. The actual value of Δd is (0, 0, 0) m, and the identified values are (−0.24, 0.06, 0.11) m as indicated in Fig. 6.

Figure 7 provides the simulation results of the three-axis attitude σ_e, and Fig. 8 provides the corresponding Euler angles (1-2-3). From Figs. 7 and 8, one can see that the convergence time of the coordinated controller is approximately 35 s, which is 10 s longer than that of the controller of thrusters only. While the tether could provide greater torque control, the pitch θ_e and yaw ψ_e angles could be controlled in a shorter time during the initial stage, and the maximum amplitudes of θ_e and ψ_e of the coordinated controller are $-43.5°$ and $-15.8°$ respectively. However, the use of thruster controller only yields the amplitude of 78.5° and $-35.1°$. An angle of 78.5° is too dangerous for the TSR system, as such a high pitch angle can lead to an entanglement of tether with the combination and cause instability in the space platform and the entire system. This result clearly demonstrates that

https://doi.org/10.1017/S0263574714000617 Published online by Cambridge University Press

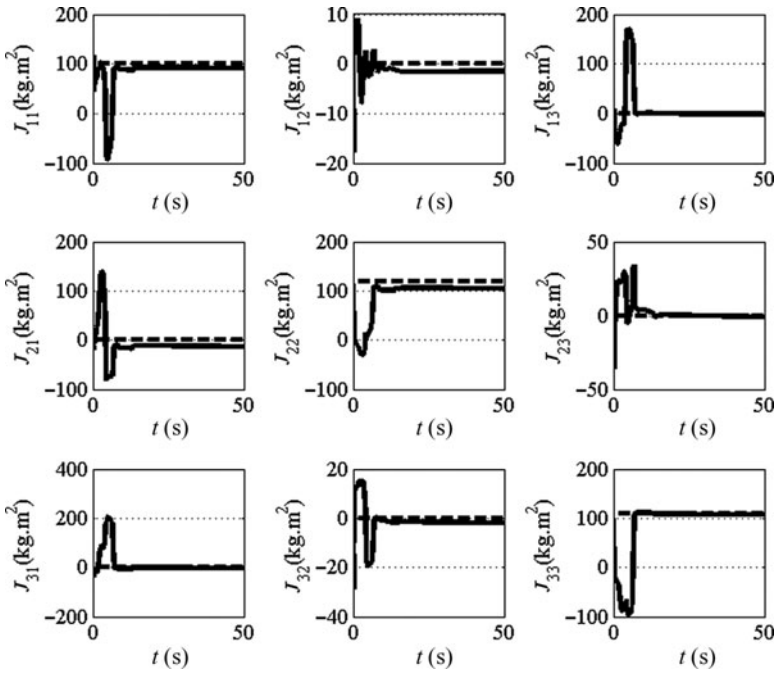


Fig. 5. Identification value of J with respect to time.

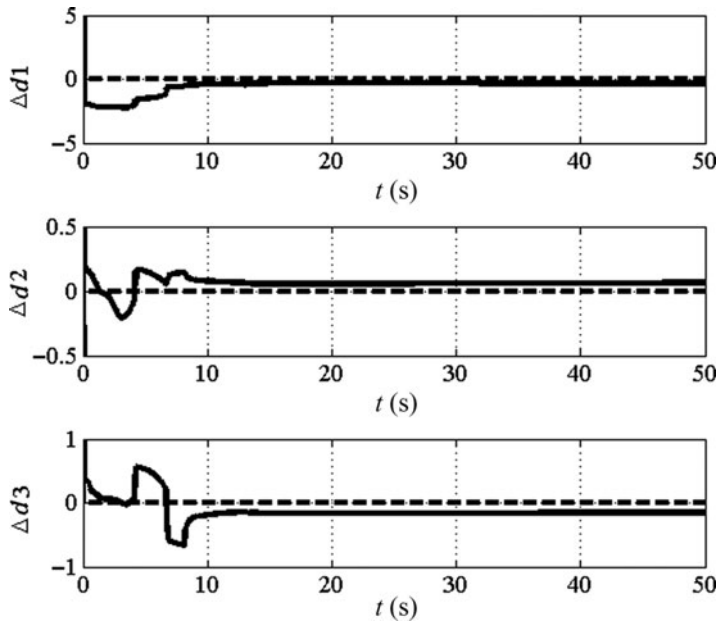


Fig. 6. Identification value of Δd with respect to time.

the use of a coordinated controller of tether and thrusters can yield smaller amplitudes of pitch θ and yaw ψ angles and lower the possibility of entanglement of tether with the combination.

An entanglement of tether typically results from the pitch and yaw angles. However, this finding does not mean that the roll motion can change freely without any control because the three-axis attitudes are coupled, and the roll motion exerts an influence on the other two motions to a certain extent. The results of a PD controller for the roll motion are provided in Fig. 8. Figure 9 shows the three-axis angular velocities of a coordinated controller and thruster controller only. The maximum

https://doi.org/10.1017/S0263574714000617 Published online by Cambridge University Press

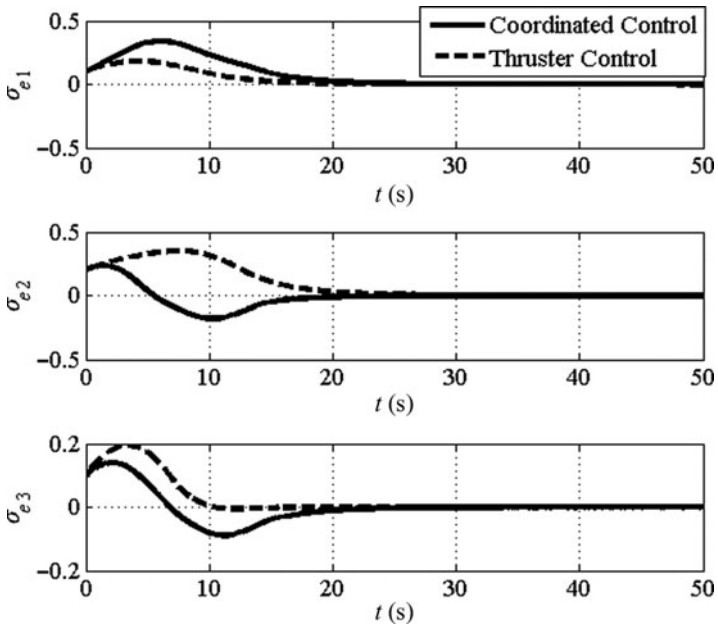


Fig. 7. Three-axis attitude, σ_e.

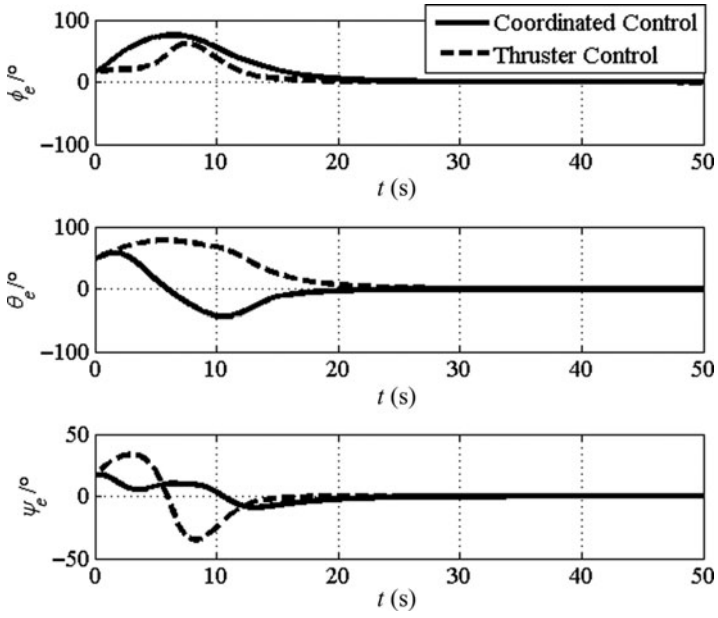


Fig. 8. Euler angles of three-axis attitude.

value of η in Fig. 10 is 58.6° , which is relatively safe for the combination system because the entanglement of tether is more likely to occur when $\eta > 90°$.

A comparison between the coordinated control of tether and thrusters and the thruster controls can be observed in Figs. 11 and 12. The second and third elements of T_c become zero for two times, and the overall control torques of the coordinated control are clearly smaller than that of the thruster control. Figures 13 and 14 demonstrate that the tether tension is utilised for two times and that the maximum torque control of the tether is approximately 18.3 Nm, which is three times bigger than that of the thruster control and could effectively lower the attitude amplitudes of the combination as shown in Figs. 7 and 8.

https://doi.org/10.1017/S0263574714000617 Published online by Cambridge University Press

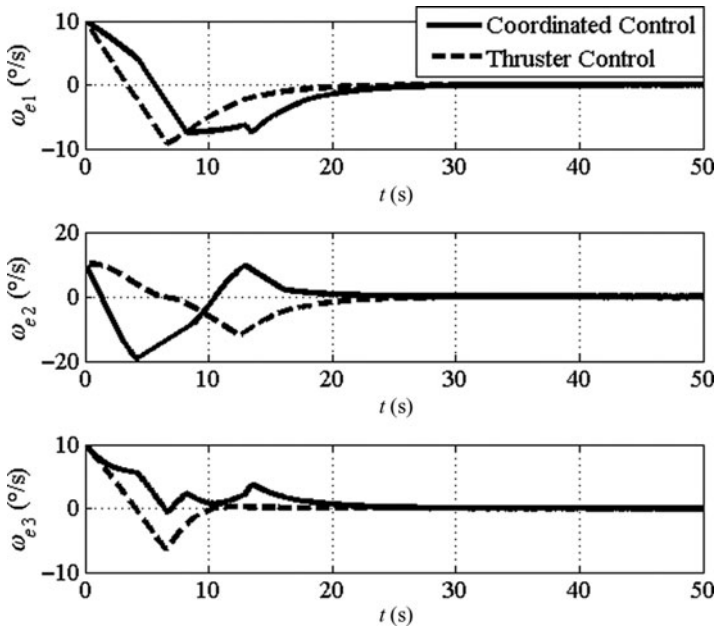


Fig. 9. Three-axis angular velocity.

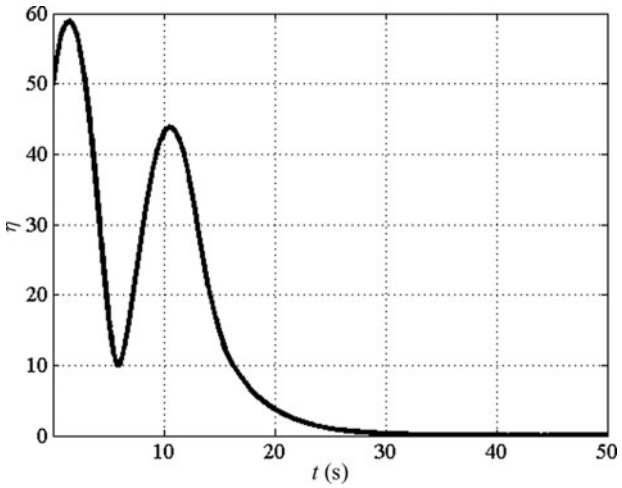


Fig. 10. Angle of η.

The fuel consumption function is defined as follows:

$$M = \int_0^{t_f} T_c^T T_c dt. \tag{34}$$

Figure 15 compares the fuel consumption of the coordinated control and the thruster control. The fuel consumption of the coordinated control consists of two parts: one part is the fuel consumption required to control the roll motion when coordinated controller is applied, and the other part is the fuel consumption of thruster controller when the switching conditions (Eq. (19)) are satisfied. The final fuel consumption of the coordinated control is 486 $N^2 \cdot m^2 \cdot s$, while that of the thruster control is

https://doi.org/10.1017/S0263574714000617 Published online by Cambridge University Press

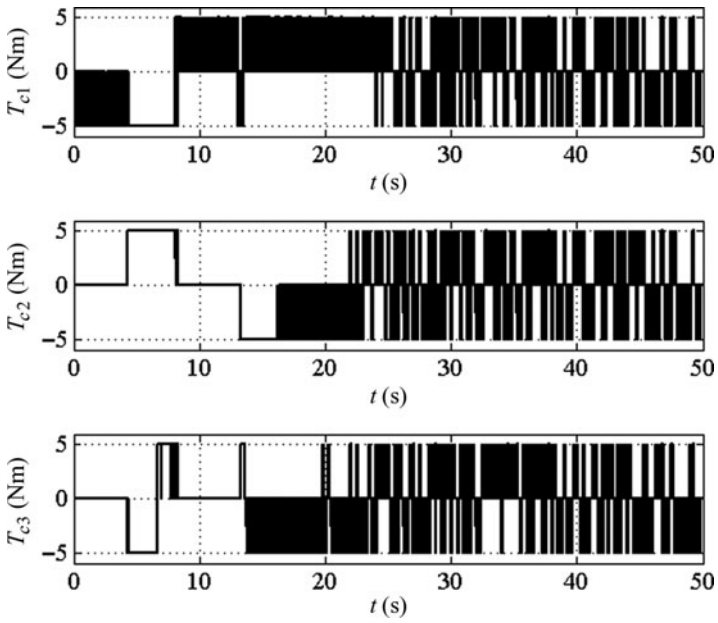


Fig. 11. Control commands of thrusters for coordinated control.

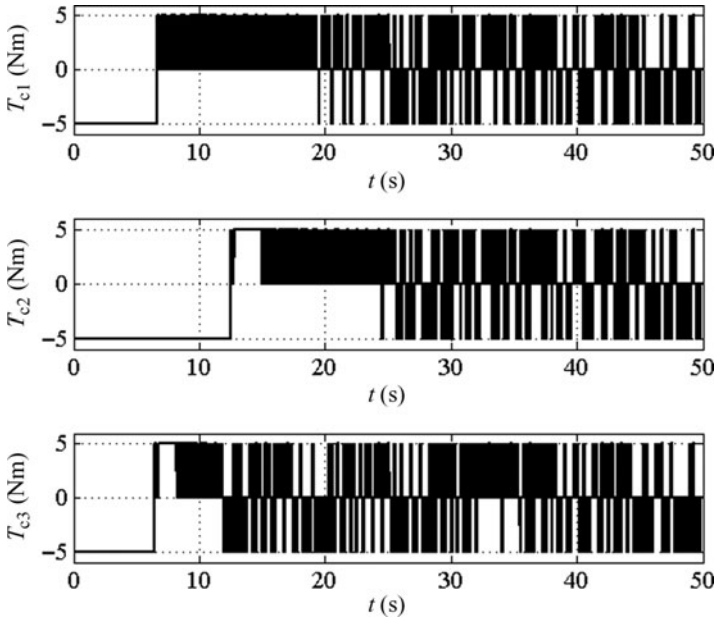


Fig. 12. Control commands of thrusters for traditional thruster control.

approximately 61.5% higher at 785 $N^2 \cdot m^2 \cdot s$, which clearly demonstrates that the coordinated control could efficiently reduce fuel consumption.

Figures 16 and 17 indicate the influence of tether tension on the combination position and linear velocity. One can see that the displacement due to the tether tension is (2.300, 0.001, 0.100) m, and the velocity change is (0.005, −0.018, 0) m/s, which are acceptable values for post-capture attitude control.

https://doi.org/10.1017/S0263574714000617 Published online by Cambridge University Press

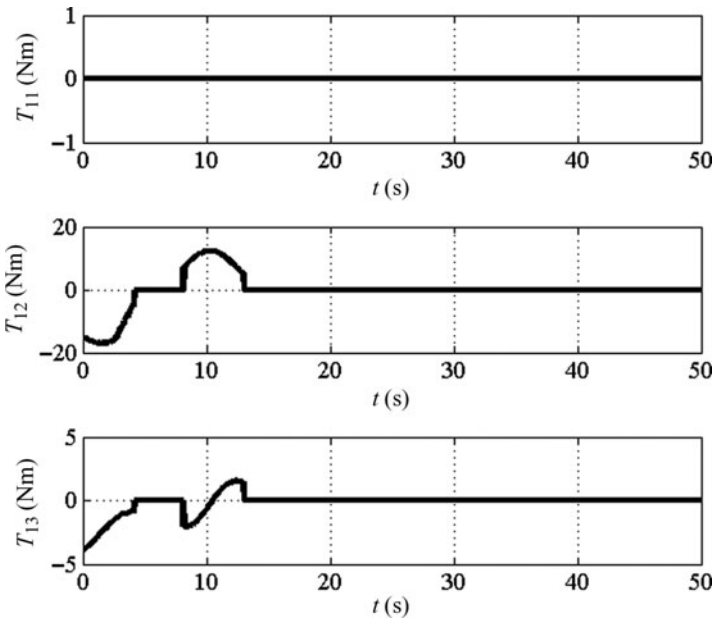


Fig. 13. Torques of tether tension.

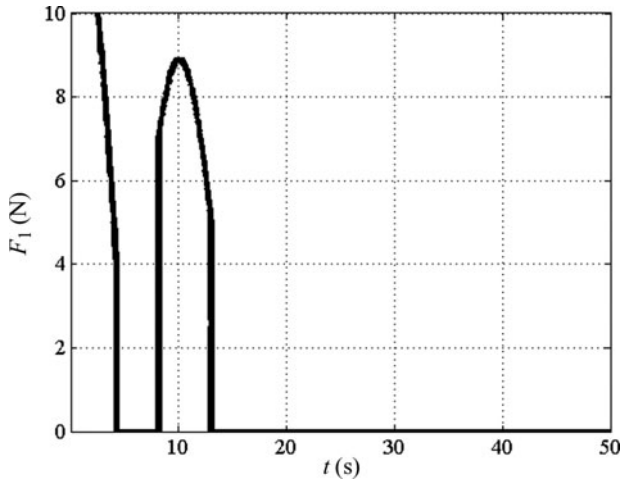


Fig. 14. Tether tension.

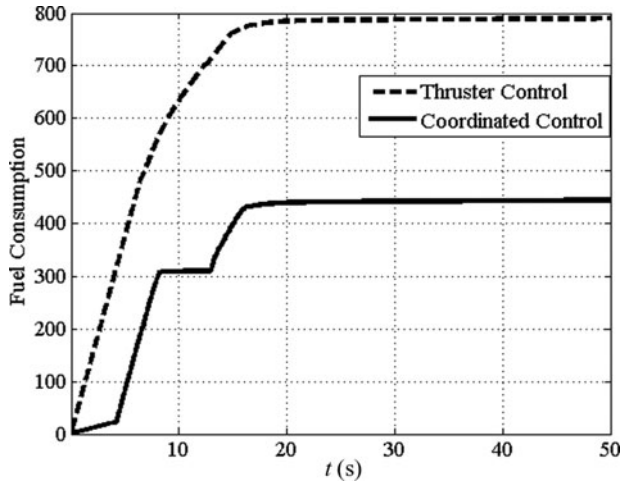


Fig. 15. Comparison of fuel consumption.

https://doi.org/10.1017/S0263574714000617 Published online by Cambridge University Press

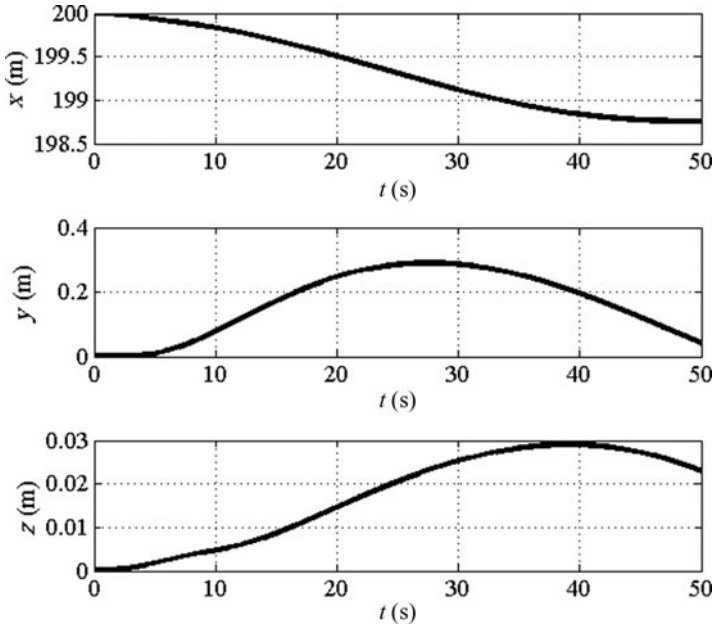


Fig. 16. Position changes due to tension.

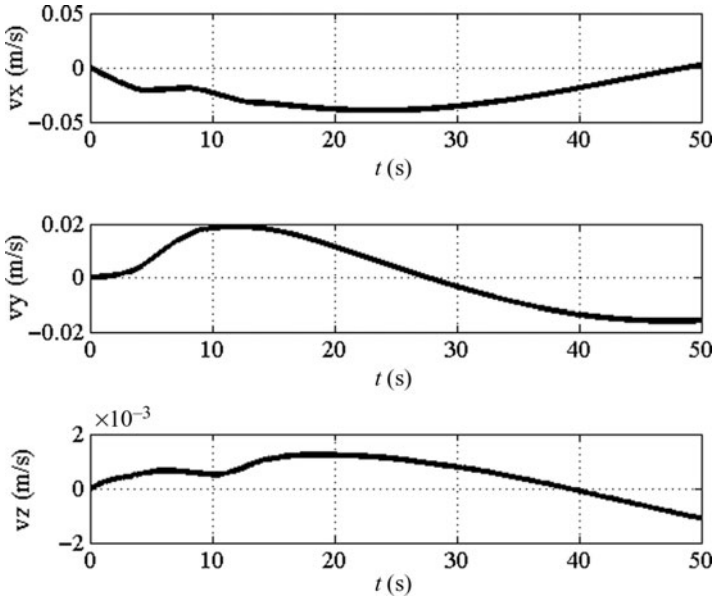


Fig. 17. Linear velocity changes due to tension.

4.2. Sensitivity analysis of attitude coordinated controller

In Section 4.1, simulation is conducted to demonstrate the advantages of the proposed coordinated control over the traditional thruster control. In this section, a simplified sensitivity analysis for different initial conditions of the combination is carried out to further validate the feasibility of this coordinated control scheme. Compared with other parameters in Table I, the initial values of attitude and angular velocity exert more influence upon the performances of the coordinated controller. Therefore, σ_e or ω_e are changed to evaluate influence on the performance of coordinated controller while other parameters involved are keep constant. Four different cases are studied as shown in Table III.

Table IV shows the simulation results of main parameters for different cases. ΔJ_{11}, ΔJ_{22} and ΔJ_{33} are the parameter identification errors of J_{11}, J_{22} and J_{33}. M_c denotes the fuel consumption of the coordinated control for each case, while M_t denotes the fuel consumption of the traditional thruster control. $(M_t - M_c)/M_c$ denotes the fuel saving rate of the coordinated controller compared

https://doi.org/10.1017/S0263574714000617 Published online by Cambridge University Press

Table III. Different cases for sensitivity analysis.

	Initial values of σ_e	Initial values of ω_e(°/s)
Case 1	(0.1, 0.3, 0.2)	(10, 10, 10)
Case 2	(0.1, 0.1, 0)	(10, 10, 10)
Case 3	(0.1, 0.2, 0.1)	(5, 5, 5)
Case 4	(0.1, 0.2, 0.1)	(15, 15, 15)

Table IV. Simulation results for different cases.

Parameters	Case 1	Case 2	Case 3	Case 4
θ_s (°)	46.1	35.7	44.5	26.1
ψ_s (°)	17.4	34.1	19.7	30.3
ΔJ_{11} (kg m^2)	−13.7	3.6	3.2	−5.2
ΔJ_{22} (kg m^2)	−14.5	0.58	−12.5	−4.1
ΔJ_{33} (kg m^2)	−2.2	5.3	5.4	3.0
Δd_1 (m)	−0.32	0.39	−0.25	−0.19
Δd_2 (m)	0.066	0.04	0.03	−0.04
Δd_3 (m)	0.003	0.21	0.10	0.16
M_c	535.2	407.1	230.4	651.4
M_t	1028.5	610.3	423.2	1622.8
$(M_t - M_c)/M_c$	92.1%	49.9%	83.7%	149.1%

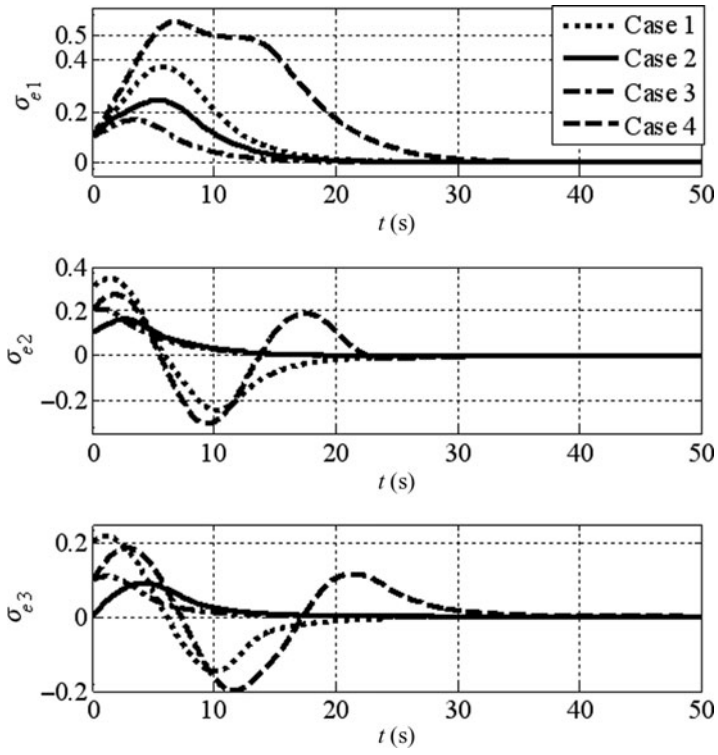


Fig. 18. Three-axis attitude σ_e of different cases.

with traditional thruster control. Parameters in Table IV are the final values of the simulations except switching conditions θ_s and ψ_s, which are obtained via parameter optimisation.

The influence of initial attitude on the performance of the coordinated attitude control is investigated via case 1, case 2 and the case in Section 4.1 with all angular velocities set as (10, 10, 10)°/s. It can be seen in Figs. 7, 8, 18 and 19 that greater initial attitude causes greater oscillation and leads to greater identification errors, as shown in Table IV. However, attitude errors of the tethered robot–target

https://doi.org/10.1017/S0263574714000617 Published online by Cambridge University Press

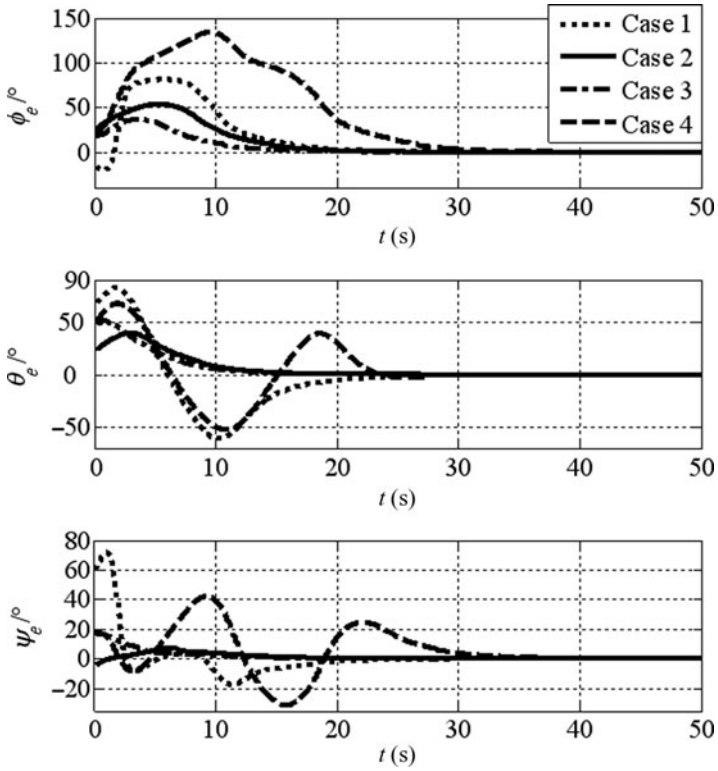


Fig. 19. Euler angles of different cases.

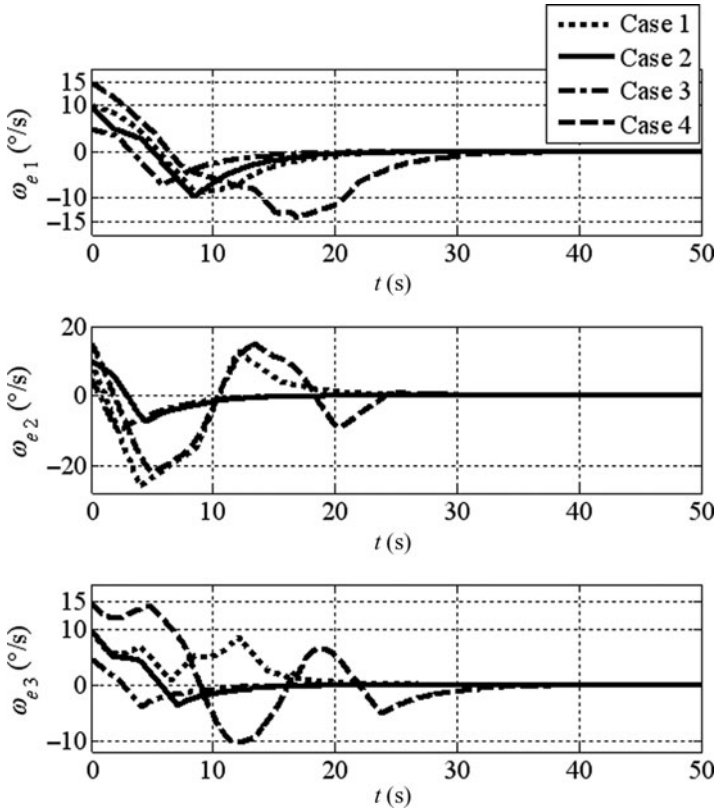


Fig. 20. Three-axis angular velocities of different cases.

https://doi.org/10.1017/S0263574714000617 Published online by Cambridge University Press

combination for each case can be effectively stabilised within 30 s. Among these three cases, case 1 has the greatest fuel consumption,, reaching 1028.5. But its effect of saving fuel consumption is most remarkable compared with the traditional thruster control, and the corresponding fuel saving rate of $(M_t - M_c)/M_c$ is 92%. It indicates that the space tether can be relatively more fully utilized when initial attitude error is greater.

Case 3, case 4 and the case in Section 4.1 are used to assess the influence of the initial spinning rate on the coordinated attitude control, and all initial attitudes are also set as constant values of (0.1, 0.2, 0.1). Figures 9 and 20 show that higher initial spinning rate of the combination leads to more oscillations during the attitude control, which are consistent with the oscillations of the attitude in Figs. 18 and 19 and 7 and 8. However, due to greater control torques provided by the space tether, these oscillations can be remarkably suppressed after 38 s and attitude errors are effectively eliminated by the coordinated controller. Compared with the thruster control of other two cases, the effect of saving fuel consumption in case 4, $(M_t - M_c)/M_c$, is highest, about 149%, which demonstrates that the performance of coordinated controller is more preferable in cases of higher spinning rates.

5. Conclusions

This paper presents a coordinated control scheme of the combination after a target is captured by a TSR. First, the dynamics models of the combination system are established. The inertial matrix and the centroid position are unknown, therefore the parameters are identified. Considering the tether can provide greater control torque than the thruster of TSR, the coordinated controllers of combination attitude are designed and the controllers are composed of two controllers that are utilised according to the switching condition. The switching condition is optimised using the genetic algorithm to ensure that the controller is stable and convergent, and to reduce fuel consumption. The numerical simulations show that the amplitudes of the pitch and yaw angles of the coordinated control are smaller than those of the traditional thruster control and could lower the possibility of entanglement of tether with the combination. Moreover, the tumbling combination can be effectively stabilised by the coordinated control. Compared with the traditional thruster control, the coordinated control strategies could efficiently reduce the fuel consumption, and the effect of saving the fuel consumption is more significant in the case of greater initial attitude or higher initial spinning rates.

Acknowledgements

This research is sponsored by the National Natural Science Foundation of China (grant No. 11272256, 61005062).

References

1. M. P. Cartmell and D. J. McKenzie, "A review of space tether research," *Prog. Aerosp. Sci*. **44**, 1–21 (2008).
2. E. M. Levin, "Dynamic analysis of space tether missions," *Adv. Astronaut. Sci*. **126**, 11–19 (2007).
3. K. D. Kumar, "Review of dynamics and control of non-electrodynamic tethered satellite systems," *J. Spacecr. Rockets* **43**(4), 705–720 (2006).
4. K. K. Mankala and S. K. Agrawal, "Dynamic modeling and simulation of impact in tether net/gripper systems," *Multibody Syst. Dyn*. **11**, 235–250 (2004).
5. P. Williams, C. Blanksby, P. Trivailo and H. A. Fujii, "In-plane payload capture using tethers," *Acta Astronaut*. **57**(10), 772–787 (2005).
6. P. Williams, "In-plane payload capture with an elastic tether," *J. Guid. Control Dyn*. **29**(4), 810–821 (2006).
7. G. Zhai, Y Qiu and B. Liang, "On-orbit capture with flexible tether-net system," *Acta Astronaut*. **65**, 613–623 (2009).
8. G. Zhai, Y. Qiu, B. Liang and C. Li, "System dynamics and feedforward control for tether-net space robot system," *Int. J. Adv. Robot. Syst*. **6**(2), 137–144 (2009).
9. M. Nohmi, T. Yamamoto and Y. Takagi, "Microgravity Experiment for Attitude Control of a Tethered Body by Arm Link Motion," *Proceedings of IEEE International Conference on Mechatronics and Automation*, Harbin (2007) pp. 3519–3524.
10. M. Nohmi, "Attitude Control of a Tethered Space Robot by Link Motion Under Microgravity," *Proceedings of the 2004 IEEE International Conference on Control Applications*, Taipei, Taiwan (2004) pp. 424–429.
11. M. Nohmi, "Mission Design of a Tethered Robot Satellite Stars for Orbital Experiment," *Proceedings of the 18th IEEE International Conference on Control Applications Part of 2009 IEEE Multi-Conference on Systems and Control Saint Petersburg*, Russia (Jul. 8–10, 2009) pp. 1075–1080.

https://doi.org/10.1017/S0263574714000617 Published online by Cambridge University Press

12. G. K. D. Kumar and B. Tan, "Nonlinear optimal control of tethered satellite systems using tether offset in the presence of tether failure," *Acta Astronaut.* **66**, 1434–1448 (May–Jun. 2010).
13. K. D. Kumar and K. Kumar, "Satellite pitch and roll attitude maneuvers through very short tethers," *Acta Astronaut.* **44**(5), 257–265 (1999).
14. P. B. Beda, "On requirements for attitude dynamics and stability control for tethered satellite systems," *JSME Int. J.* **43**(3), 678–683 (2000).
15. O. Mori and S. Matunaga, "Formation and attitude control for rotational tethered satellite," *J. Spacecr. Rockets* **44**(1), 211–220 (2007).
16. I. Chang, S.-Y. Park and K.-H. Choi, "Nonlinear attitude control of a tether-connected multi-satellite in three-dimensional space," *IEEE Trans. Aerosp. Electron. Syst*. **46**(4), 10 (2010).
17. C. Menon and C. Bombardelli, "Self-stabilizing attitude control for spinning tethered formations," *Acta Astronaut*. **60**, 828–833 (2007).
18. S. Bergamaschi and F. Bonon, "Coupling of tether lateral vibration and sub-satellite attitude motion," *J. Guid Control Dyn*. **15**(5), 1284–1286 (1992, Sep.–Oct.).
19. K. Yoshida, D. Dimitrov and H. Nakanishi, "On the Capture of Tumbling Satellite by a Space Robot," *Proceedings of the 2006 IEEE/RSJ International Conference on Intelligent Robots and Systems*, Beijing, China (2006) pp. 4127–4132.
20. A. Flores-Abad and O. Ma, "Control of a Space Robot for Minimal Attitude Disturbance to the Base Satellite for Capturing a Tumbling Satellite," *SPIE Proceedings on Sensors and System for Space Applications*, Vol. 8385, 83850J-1 (2012).
21. S. Liu, L. Wu and Z. Lu, "Impact dynamics and control of a flexible dual-arm space robot capturing an object," *Appl. Math. Comput.* **185**, 1149–1159 (2007).
22. T. Chau, N. Huynh and I. Sharf, "Adaptive Reactionless Motion with Joint Limit Avoidance for Robotic Capture of Unknown Target in Space," *2012 IEEE/RSJ International Conference on Intelligent Robots and Systems*, Vilamoura, Algarve, Portugal (2012) pp. 1155–1160.
23. F. Aghili, "Optimal Control of a Space Manipulator for Detumbling of a Satellite," *International Conference on Robotics and Automation*, Kobe, Japan (May 12–17, 2009) pp. 3019–3024.
24. F. Aghili, "Coordination Control of a Free-Flying Manipulator and its Base Attitude to Capture and Detumble a Noncooperative Satellite," *2009 IEEE-RSJ International Conference on Intelligent Robots and Systems* (2009) pp. 2365–2372.
25. W. Xu, C. Li, B. Liang, Y. Xu et al., "Target berthing and base reorientation of free-floating space robotic system after capturing," *Acta Astronaut.* **64**, 109–126 (2009).
26. N. Yuya, S. Fumiki and N. Shinichi, *Guidance and Control of "Tethered Retriever" with Collaborative Tension-Thruster Control for Future On-Orbit Service Missions* (Special Publication) (European Space Agency, ESA SP, Paris, France, 2005.
27. D. B. Spencer, D. B. Seybold, A. K. Misra and R. J. Lisowski, "Dynamics and control of a tethered space robot with tension," *Adv. Astronaut. Sci*. **109**, 1587–1595 (2001).
28. K. K. Mankala and S. K. Agrawal, "Dynamic modeling and simulation of satellite tethered systems," *J. Vib. Acoust*. **127**, 144–156 (2005).
29. J. L. Crassidis and F. L. Markley, "Sliding mode control using modified Rodrigues parameters," *J. Guid. Control Dyn.* **19**(6), 1381–1383 (1996).
30. G. Q. Xing and S. A. Parvez, "Nonlinear attitude state tracking control for spacecraft," *J. Guid. Control Dyn.* **24**(3), 624–626 (2001).
31. M. Srinivas and L. M. Patnaik, "Genetic algorithms: A survey," *Computer* **27**(6), 17–26 (1994).

https://doi.org/10.1017/S0263574714000617 Published online by Cambridge University Press